Journal of Sound and Vibration (2001) **248**(5), 829–845
doi:10.1006/jsvi.2001.3815, available online at http://www.idealibrary.com on IDEAL®

CYCLOSTATIONARY ANALYSIS OF ROLLING-ELEMENT BEARING VIBRATION SIGNALS

I. Antoniadis and G. Glossiotis

Department of Mechanical Engineering, Machine Design and Control Systems Section, National Technical University of Athens, P.O. Box 64078, *Athens* 15710, *Greece.*
E-mail: antogian@central.ntua.gr

(*Received* 20 *September* 2000, *and in final form* 9 *March* 2001)

Vibration signals resulting from rolling-element bearings present a mixture of physical information, the proper analysis of which can lead to the identification of possible faults. Traditionally, this analysis is performed by the use of signal processing methods, which assume statistically stationary signal features. The paper proposes an alternative framework for analyzing bearing vibration signals, based on cyclostationary analysis. This framework, being able to model, additionally, signals with periodically varying statistics, is better able to exhibit the underlying physical concepts of the modulation mechanism present in the vibration response of bearings. The basic concepts of the approach are demonstrated both in illustrative simulation results, as well as in experimental results and industrial measurements for two different types of bearing faults.

1. INTRODUCTION

Due to the fact that rolling-element bearings are one of the most important and frequently encountered components in the vast majority of rotating machines, the analysis of their vibration response has over the years been the subject of extensive research. Bearing defects or wear cause impacts at frequencies governed by the operating speed of the unit and the geometry of the bearings, which in turn excite various machine natural frequencies. This physical effect has been exploited by several vibration analysis methods [1], based either on detailed models of the vibration response, or on signal processing methods.

A comprehensive model for the nature of vibrations induced by a single point defect in a rolling-element bearing has been proposed in reference [2]. Several other models, taking more detailed account of physical effects such as imperfections, wear or lubrication have been proposed in references [3–5]. The general baseline of all those models, is the fact that the measured signal contains a low-frequency phenomenon that acts as a modulator to a high-frequency carrier signal. The low-frequency phenomenon is the excitation pattern caused by the fault or the imperfection of the bearing, while the high-frequency carrier is a combination of the natural frequencies of the associated rolling element or even of the machine.

Several signal processing methods have been developed to extract the useful information contained in the measured signal from the overall vibration response. Most methods consider the signal statistical properties as stationary. A typical well-established example is the demodulation or enveloping method, a typical implementation of which is presented in reference [6]. This method is based on traditional spectral analysis, properly combined with the Hilbert transform, in order to isolate the envelope of the measured signal from the rest of the signal features.

0022-460X/01/500829 + 17 $35.00/0

However, in the case of bearing vibration signals, and more generally in rotating machine vibration analysis, the overall response is a combination of periodic components, dominated by the machine rotation, with signals of a random nature, dominated by a possible bearing fault or imperfection. Due to the periodic nature of the phenomena involved, time invariance and consequently, the notion of stationary is violated in practice.

This fact has led to the development of a number of time–frequency analysis methods, such as the short-time Fourier transform (STFT), the Wigner–Ville distribution (WVD) or the wavelet transform (WT), the latter having been established as the most widespread joint time–frequency analysis tool due, among other factors, to its inherent capability to be realized in real-time in the form of a discrete wavelet transform (DWT). The WT has already been used with success in specific case studies for bearing fault detection [7–9].

An alternative framework for analyzing periodically time-varying signals is based on cyclostationary analysis. In contrast to the conventional statistical signal processing methods that treat random signals assuming stationary statistics, cyclostationary analysis assumes periodically time-varying statistics [10, 11]. Preliminary results of the application of cyclostationary analysis to specific machine components are presented in references [12, 13].

This paper proposes the application of cyclostationary analysis to vibration signals from rolling-element bearings. The main emphasis of the paper is on the proper exploitation by cyclostationary analysis of the physical mechanism that generates the vibration response, taking into full account its underlying physical concepts and major conclusions. Section 2 of the paper summarizes the basic concepts and theory of cyclostationary analysis. Section 3 provides illustrative examples of cyclostationary analysis of indicative signals, including signals simulating bearings with an inner and an outer race fault. Industrial measurements and experimental results for two different types of bearing faults are provided in section 4, verifying the effectiveness of the method.

2. BASIC CONCEPTS OF CYCLOSTATIONARY ANALYSIS

2.1. DEFINITIONS

The concept of *cyclostationarity* (cyclic stationarity) has existed for almost 40 years [10, 11]. Apart from this term, many others have been introduced, such as *periodically correlated*, *cycloergodic*, *periodically stationary*, etc. According to the strict definition, a random process $x(t)$ is cyclostationary of order N with period T, if for every $n = 1, N$ and time instants $t_1, t_2, \ldots, t_n$, the probability distribution function $P_{x(t)}$ is periodic with period T:

$$P_{x(t)} = P_{x(t+T)}, \tag{1a}$$

$$P_{x(t)} \equiv Prob\{x(t + t_1) \leqslant X_1, x(t + t_2) \leqslant X_2, \ldots, x(t + t_n) \leqslant X_n\}. \tag{1b}$$

As a direct consequence of equation (1), the moments and cumulants of $x(t)$ also vary periodically with time:

$$\mathrm{E}\left\{\prod_{i=1}^{N} x(t_i)\right\} = \mathrm{E}\left\{\prod_{i=1}^{N} x(t_i + T)\right\}, \tag{2}$$

where N denotes the order of the statistic function and $\mathrm{E}\{\cdot\}$ denotes the statistical expectation operator. Provided that only equation (2) is valid, the random process $x(t)$ is cyclostationary only in a wide sense.

Assuming also that the process is *cycloergodic* [10], the statistical expectation operator $E\{\cdot\}$ in equation (2) can be replaced by the time average operator $\langle\cdot\rangle$, which can be equivalently defined either in its continuous, or in its discrete form as

$$\langle x(t)\rangle \equiv \underbrace{\lim}_{T\to\infty} \frac{1}{2T}\int_{-T}^{T} x(t)\,\mathrm{d}t, \tag{3a}$$

$$\langle x(n)\rangle \equiv \underbrace{\lim}_{M\to\infty} \frac{1}{(2M+1)}\sum_{j=-M}^{M} x(j). \tag{3b}$$

In the remaining part of the paper, only wide-sense cyclostationary cycloergodic processes with an order of up to two will be considered.

2.2. FIRST ORDER CYCLOSTATIONARITY

A first order cyclic statistical process, $N = 1$, can be efficiently represented by the time periodical mean (first order moment):

$$m(t) = \mathrm{E}\{x(t)\} = m(t+T). \tag{4}$$

An example of a first order cyclostationary process is a sinusoidal signal with added Gaussian noise:

$$x(t) = a\cos(2\pi f_0 t + \theta) + s(t). \tag{5}$$

The noise $s(t)$ clearly causes the signal to be random. If the signal is averaged by matching up points from the same position each time in the cycle (synchronous averaging), then the underlying sinusoid will be recovered. However, if the variance of the signal is computed in the same way, it will be found to be constant.

First order cyclostationary is exploited in condition monitoring applications through the use of rotation synchronous averaging [13]. According to this method, a vibration signal $x(t)$ is averaged for one rotation period by calculating the mean of the samples that have been measured for a number of rotations N separated by a time interval T of one period of rotation:

$$m(t) = \frac{1}{(N-1)}\sum_{l=0}^{N-1} x(t+lT). \tag{6}$$

This process produces a single period of a deterministic periodic signal (the first order cyclic moment) which can then be decomposed into its Fourier series coefficients using the Fourier transform. Afterwards, the synchronous averaged signal can be further exploited by other condition monitoring methods such as amplitude or phase demodulation, wavelet decomposition, etc.

2.3. SECOND ORDER CYCLOSTATIONARITY

The second order theory of cyclostationary signals deals with the autocorrelation function:

$$R_x(t, t-\tau) = R_x(t,\tau) = \mathrm{E}\{x(t)x(t-\tau)\}. \tag{7}$$

According to the definition of cyclostationary signals, this function of the signal $x(t)$ is periodic in t for each time shift τ:

$$R_x(t, \tau) = R_x(t + kT, \tau), \quad k = 0, 1, 2, \ldots. \tag{8}$$

Since the above function is periodic, it can be expanded into a Fourier series:

$$R_x(t, t - \tau) = \sum_{\{\alpha\}} R_x^{\alpha}(\tau) \mathrm{e}^{\mathrm{j}2\pi\alpha(t - \tau/2)}. \tag{9}$$

The Fourier coefficients of the above periodic time-varying autocorrelation function define the *cyclic autocorrelation function*:

$$R_x^{\alpha}(\tau) = \mathrm{E}\{x(t)x(t - \tau)\mathrm{e}^{-\mathrm{j}2\pi\alpha(t - \tau/2)}\}. \tag{10}$$

An equivalent form for equations (8) and (10) is obtained, if the autocorrelation is given in a symmetric form, centred at time t:

$$R_x(t, \tau) = \mathrm{E}\{x(t - \tau/2)x(t + \tau/2)\}, \tag{11}$$

$$R_x^{\alpha}(\tau) = \mathrm{E}\left\{x\left(t - \frac{\tau}{2}\right)x\left(t + \frac{\tau}{2}\right)\mathrm{e}^{-\mathrm{j}2\pi\alpha t}\right\}. \tag{12}$$

In the above equations, the quantity $\alpha = 1/T$ is defined as the *cycle frequency* or *frequency separation.*

The cyclic autocorrelation function provides an indication of how much energy in the signal is due to cyclostationary components at frequency α. Along the line $\alpha = 0$, the function $R_x^{\alpha}(\tau)$ reduces to the conventional autocorrelation function. Based on this observation, the significant amount of energy existing along lines where $\alpha \neq 0$, indicates that the signal is second order cyclostationary. This implies that the amplitude and/or phase fluctuations of some narrow-band frequency components of the signal with centre frequencies that are separated by a non-zero amount are temporally correlated. The frequency separations of these correlated spectral components are specified by distinct values of the cycle frequency α, where a significant amount of energy of the signal is present.

As a first measure of the existence of cyclostationary components in a signal, the *degree of cyclostationarity* (DCS) function of the signal can be used, defined, respectively, for continuous and for discrete signals as follows:

$$DCS^{\alpha} = \frac{\int_{-\infty}^{+\infty} |R_x^{\alpha}(\tau)|^2 \, \mathrm{d}\tau}{\int_{-\infty}^{+\infty} |R_x^{0}(\tau)|^2 \, \mathrm{d}\tau}, \tag{13a}$$

$$DCS^{\alpha} = \frac{\sum_{\tau} |R_x^{\alpha}(\tau)|^2}{\sum_{\tau} |R_x^{0}(\tau)|^2}. \tag{13b}$$

However, far more insight into the cyclostationary features of the signal can be provided by the usage of the *spectral correlation density function* (SCDF) of the signal. Similar to the way that the power spectral density (PSD) function of a signal can be obtained by the Fourier transform of its stationary autocorrelation function, the SCDF can be calculated by the Fourier transform of the cyclic autocorrelation function, with respect to

the time shift τ:

$$S_x^\alpha(f) = S_x(a,f) = \int_{-\infty}^{\infty} R_x^\alpha(\tau) e^{-j2\pi f\tau} d\tau. \tag{14}$$

By properly transforming equation (12), the SCDF can be shown [10] to be equivalently expressed as

$$S_x(a,f) = E\{X(f-\alpha/2)X^*(f+\alpha/2)\}, \tag{15}$$

where $X(f)$ is the Fourier transform of $x(t)$.

It can be readily observed from equation (15) that the SCDF reduces to the conventional PSD along the line $\alpha = 0$. The SCDF provides the correlation between spectral components centred on a frequency f and separated by a frequency shift of $\alpha/2$. Based on the symmetry properties of the Fourier transform, it can be shown that the SCDF also possesses symmetric properties along the axes $f = 0$ and $a = 0$ and also along the line defined by the points $f = fs/2$, $a = fs$, where fs is the sampling frequency of the signal.

Using equation (14), equation (13) can be written in the following equivalent form:

$$DCS^\alpha = \frac{\int_{-\infty}^{+\infty} |S_f^\alpha(f)|^2 df}{\int_{-\infty}^{+\infty} |S_f^0(f)|^2 df}, \tag{16a}$$

$$DCS^\alpha = \frac{\sum_f |S_f^\alpha(f)|^2}{\sum_f |S_f^0(f)|^2}. \tag{16b}$$

Equation (16) implies that the presentation of the DCS function is just as simple as the presentation of the PSD of the envelope of the signal. However, the computation of the DCS function according to equation (16) is far more straightforward than the computation of the PSD of the envelope of the signal, eliminating the various implications, which can result in the existing demodulation methods. A further advantage of the DCS function raises from the fact that it presents a non-dimensional quantity, which can be used more effectively for fault trend analysis.

Many efficient algorithms have been developed for the estimation of the SCDF, based on classical cross-spectra estimation methods [11, 14]. In general, two estimation alternatives are available: (1) The smoothed cyclic periodogram: (2) the smoothed cyclic correlogram. The cyclic periodogram can be in turn smoothed either spectrally or temporally.

3. EXAMPLES OF CYCLOSTATIONARY ANALYSIS

In order to clarify how the cyclostationary features are introduced in a signal, as well as the advantages of cyclostationary analysis compared to the conventional spectral analysis, a number of simulated signals will be analyzed.

3.1. HARMONIC SIGNALS IN MULTIPLICATIVE NOISE

The first example considers an amplitude modulated signal in the form

$$x(t) = a(t)\cos(2\pi f_0 t), \tag{17}$$

where $a(t)$ is a real stationary random signal with zero mean and with a PSD $S_a(f)$ which contains no spectral lines:

$$\langle a(t)\rangle = 0, \qquad \langle a(t)a^*(t-\tau)\rangle \neq 0, \tag{18a, b}$$

$$\langle a(t)a^*(t-\tau)\mathrm{e}^{-\mathrm{j}2\pi\alpha t}\rangle = 0 \quad \text{for all } \alpha \neq 0. \tag{18c}$$

The detailed cyclostationary analysis of this signal is performed in reference [10]. The PSD $S_x(f)$ of the amplitude modulated signal $x(t)$ is given by

$$S_x(f) = \tfrac{1}{4}S_a(f+f_0) + \tfrac{1}{4}S_a(f-f_0). \tag{19}$$

It is obvious that no spectral lines appear in the PSD spectrum at the frequency f_0 or $-f_0$.

However, obtaining the square of the signal $x(t)$, the PSD $S_y(f)$ of the resulting signal $y(t)$ is given by

$$S_y(f) = \tfrac{1}{4}[S_b(f) + \tfrac{1}{4}S_b(f+2f_0) + \tfrac{1}{4}S_b(f-2f_0)]. \tag{20}$$

which now contains spectral lines at the frequencies $f = \pm 2f_0$ as well as at $f = 0$. The reason for this is that the DC component of the signal $b(t)$ is non-zero, contrary to the DC component of the signal $a(t)$, which is zero.

Thus, by applying a quadratic transformation (a square in this case), to the original signal $x(t)$, the hidden periodicity resulting from the sine wave factor $\cos(2\pi f_0 t)$ in equation (17) is converted into first order periodicity with associated spectral lines.

Applying cyclostationary analysis to the signal $x(t)$, its cyclic autocorrelation function and the corresponding SCDF are correspondingly:

$$R_x^\alpha(\tau) = \begin{cases} \tfrac{1}{4}R_a(\tau) & \text{for } \alpha = \pm 2f_0, \\ \tfrac{1}{2}R_a(\tau)\cos(2\pi f_0\tau) & \text{for } \alpha = 0, \\ 0 & \text{otherwise,} \end{cases} \tag{21}$$

$$S_x^\alpha(f) = \begin{cases} \tfrac{1}{4}S_a(f) & \text{for } \alpha = \pm 2f_0, \\ \tfrac{1}{4}S_a(f+f_0) + \tfrac{1}{4}S_a(f-f_0) & \text{for } \alpha = 0, \\ 0 & \text{otherwise,} \end{cases} \tag{22}$$

where $R_a(\tau)$ and $S_a(f)$ are the autocorrelation function and the PSD function of the signal $a(t)$. Thus, the cycle spectrum consists of only the two cycle frequencies $\alpha = \pm 2f_0$ and the degenerate cycle frequency $\alpha = 0$.

The cyclostationary analysis of a number of typical signal patterns is presented in references [10, 11]. Figure 1 shows the SCDF of the sum of two cosine signals modulated and with white noise added. The values of the SCDF on the spectral frequency f-axis correspond to the traditional PSD of the signal and clearly reveal peaks at the signal frequencies. A similar pattern appears on the cycle frequency α-axis, with the difference now, that in view of equation (21), the peaks appear at double the signal frequencies. Moreover, the SCDF pattern is characterized by peaks at the sum and difference of the two frequencies.

3.2. SIGNALS SIMULATING ROLLING-ELEMENT BEARING VIBRATION RESPONSE

According to a number of well-established models, [2–5], a bearing defect or imperfection striking one of the rolling elements produces an impact, the magnitude of

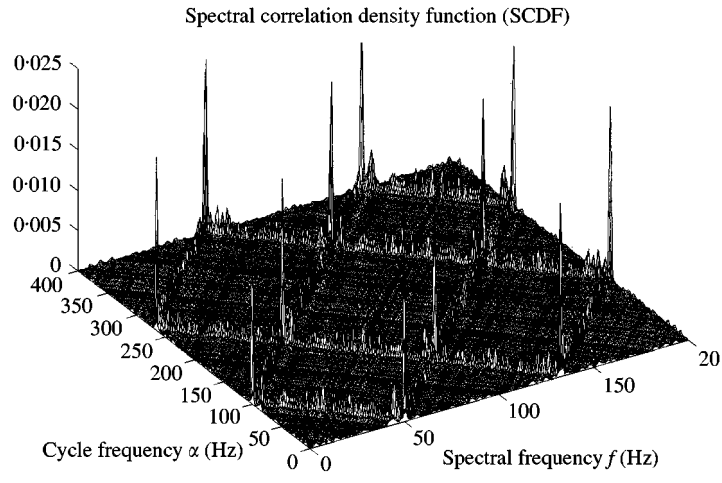

Figure 1. Spectral correlation density function of the sum of two cosine signals with corresponding frequencies at 50 and 133 Hz. The signals are modulated and added to white noise.

which is dependent on the severity of the wear and also on the load on the defect at the time of impact. As the bearing rotates, the impacts occur periodically at frequencies characterized by the nature of the fault, the rotation speed and the bearing geometry [1]. This excitation force, dependent on its location and spectral content, excites a number of machine natural frequencies. Thus, the total bearing vibration response pattern is typically characterized by trains of periodically repeated and strongly modulated components.

In view of the analysis in section 2.2 of the paper, cyclostationary analysis can provide an effective tool for the proper identification and the correlation of the several modulation mechanisms present in the signal. As a first step, two types of simulated signals are considered, representing, respectively, the simplified typical rolling-element bearing vibration responses in the case of an outer and an inner race bearing fault. Additionally, to provide further insight into the concepts of cyclostationarity, the purpose of the analysis of these signals is the identification of typical "frequency patterns" that are present both in the DCS and the SCDF functions of the signal and uniquely exhibit the modulation effects, which can characterize each type of bearing fault.

The first simulated signal used is shown in Figure 2. The signal contains the basic features of a typical vibration response, generated by an outer race bearing fault with a ball passing frequency outer race (BPFO) of 125 Hz and a structural natural frequency of 1000 Hz. The PSD of the signal in Figure 3 indicates a number of distinct frequencies, presumably sidebands around the central frequency of 1000 Hz. The DCS of the signal, resulting form equation (16), is presented in Figure 4. It is characterized by the presence of a number of non-zero cycle frequencies A1–A4, corresponding, respectively, to the BPFO frequency of the signal and its harmonics. This provides a first indication that a modulation effect is present in the signal.

Further information about the exact form of the modulation mechanism present in the signal is provided by the SCDF shown in Figure 5. The SCDF is characterized by the clear presence of a number of distinct points. All the points of the SCDF lie in skew lines, originating from the distinct points present on the spectral frequency axis f, which correspond to the values of the distinct frequencies of the PSD function of the signal. These points define a symmetric rhombic structure around the vertical axis, originating at the

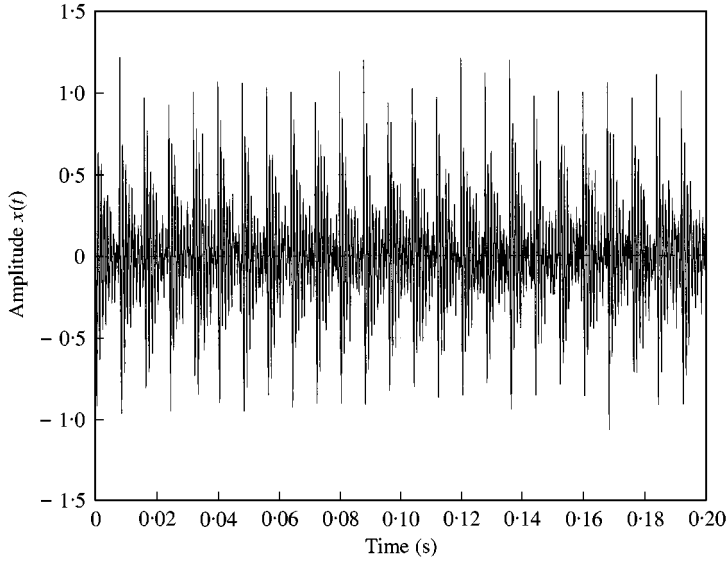

Figure 2. Periodic train of damped harmonic components added in noise, simulating bearing response under an outer race fault. The damped components have a frequency of 1000 Hz and a repetition frequency of 125 Hz.

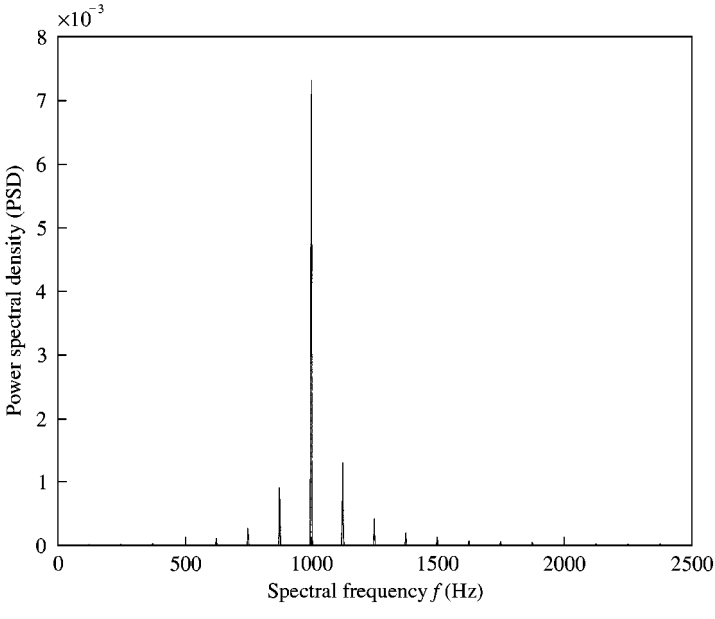

Figure 3. Power spectral density of the signal in Figure 2.

natural frequency of 1000 Hz. The spacing of the points is the BPFO frequency of 125 Hz in the horizontal direction and double this in the vertical direction.

In view of the analysis in section 2.2, this pattern of the SCDF function provides clear evidence of the correlation of the natural frequency of 1000 Hz with the BPFO frequency of 125 Hz. This correlation verifies the specific modulation effect present in the signal.

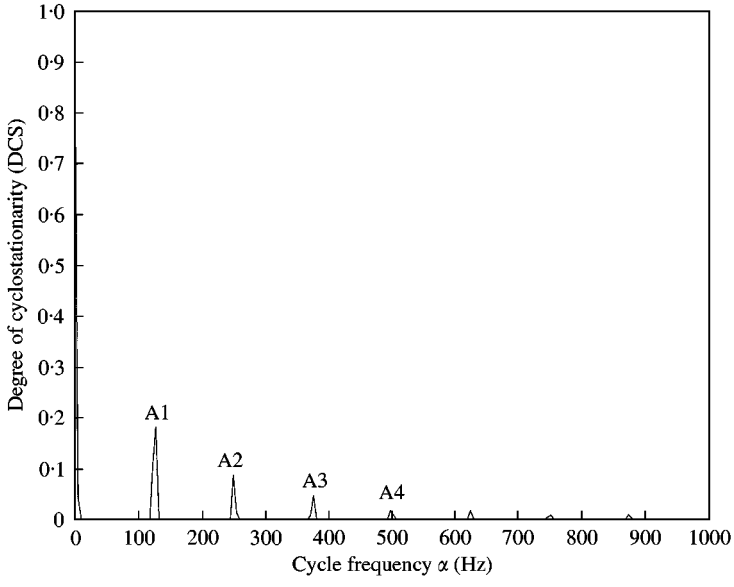

Figure 4. Degree of cyclostationarity function of the signal in Figure 2.

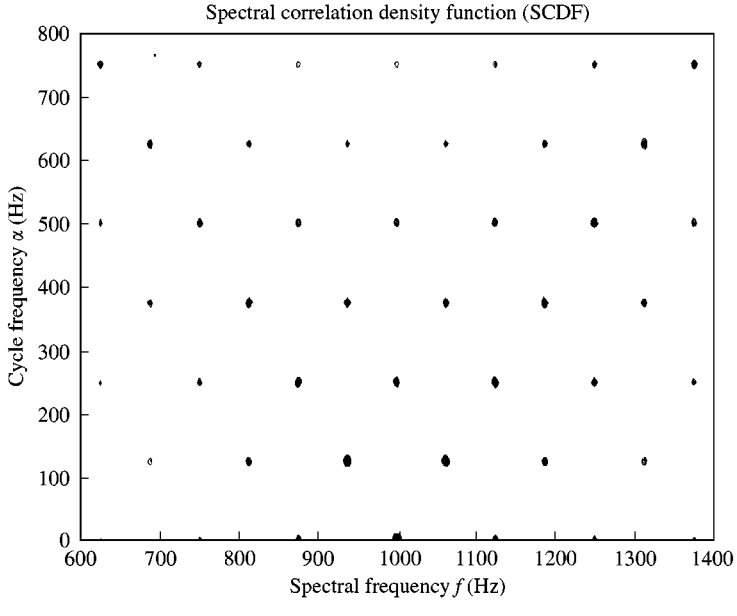

Figure 5. Spectral correlation density function of the signal in Figure 2.

Moreover, the patterns appearing in the DCS function and the SCDF (Figures 4 and 5, respectively), provide corresponding typical "frequency patterns" to be expected in bearing vibration signals under an outer race fault.

Figure 6 presents a similar pulse train, the total amplitude of which is in this case further modulated with an additional harmonic component. The signal contains the basic features

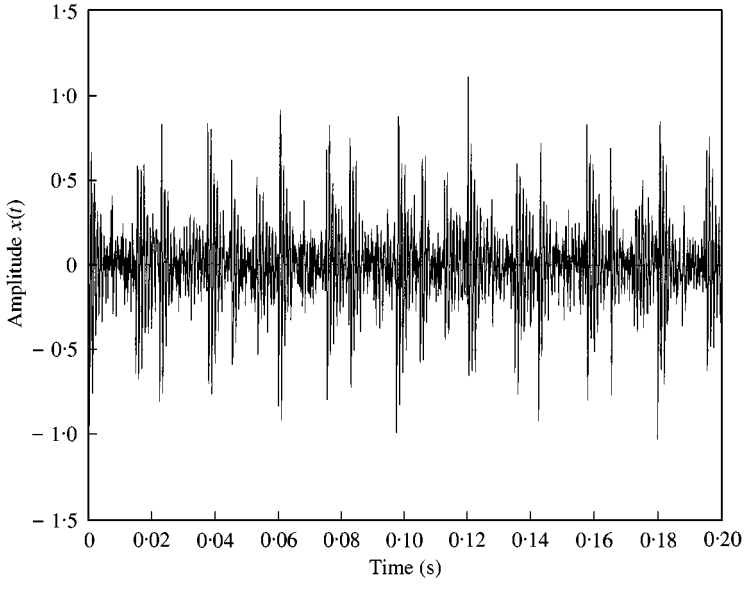

Figure 6. Periodic train of damped harmonic components added noise, simulating bearing response under an inner race fault. The damped components have a frequency of 1000 Hz, a repetition frequency of 133 Hz and an overall amplitude modulation frequency of 25 Hz.

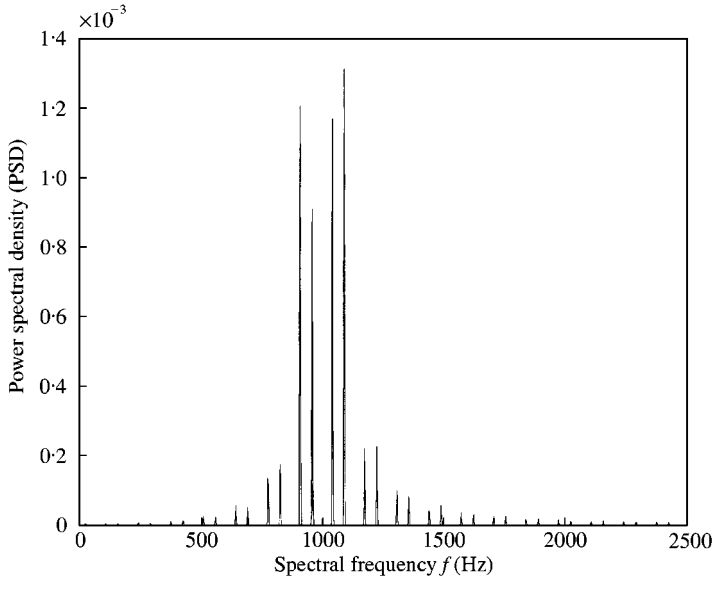

Figure 7. Power spectral density of the signal in Figure 6.

of a typical vibration response, generated by an inner race bearing fault with a ball passing frequency inner race (BPFI) of 133 Hz, a structural natural frequency of 1000 Hz and a shaft rotation frequency of 25 Hz. The PSD of the signal in Figure 7, far more complex in structure than that of Figure 3, indicates a number of distinct frequencies around the central frequency of 1000 Hz. The DCS of the signal is presented in Figure 8. The distinct

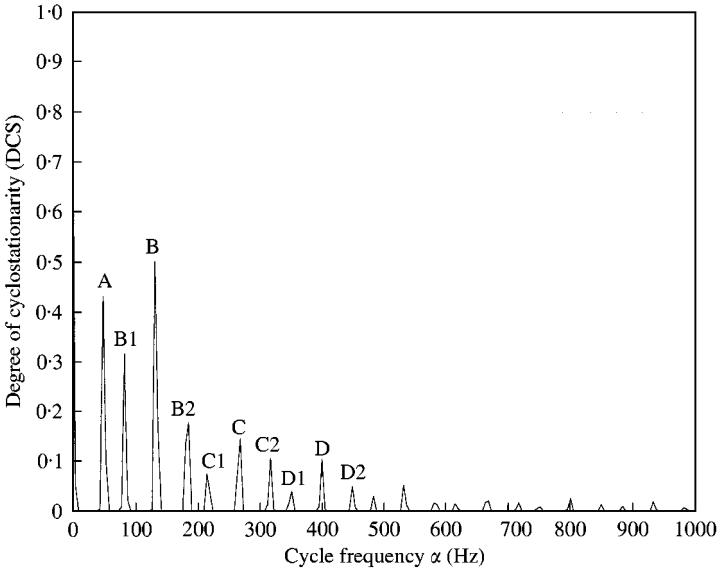

Figure 8. Degree of cyclostationarity function of the signal in Figure 6.

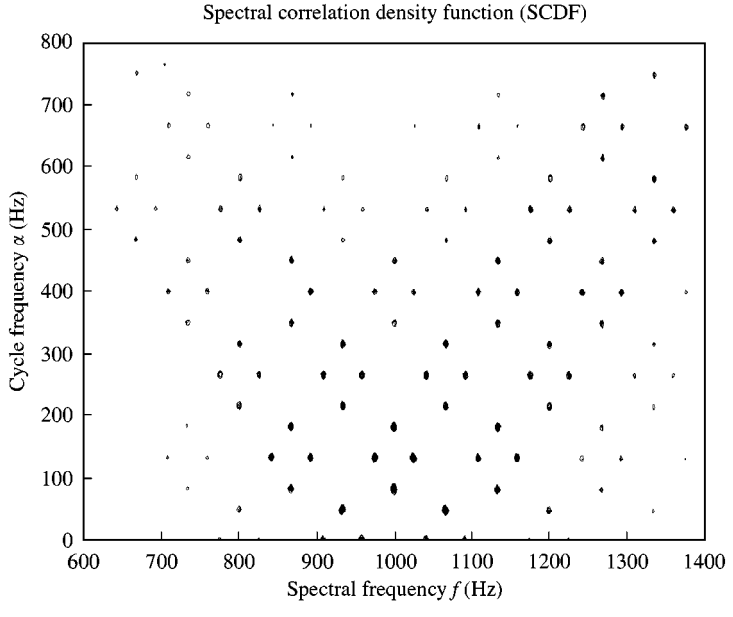

Figure 9. Spectral correlation density function of the signal in Figure 6.

cycle frequencies correspond to double the shaft rotation speed of 25 Hz, (point A), to the BPFI frequency and its harmonics (points B, C, D, respectively) and to sidebands around them (points B1–B2, C1–C2, D1–D2, respectively) at frequencies equal to double the shaft rotation speed.

The SCDF of the signal is presented in Figure 9. The SCDF is again characterized by the clear presence of a number of distinct points in skew lines, originating from the points on the spectral frequency axis f, which correspond to the values of the peak frequencies of the PSD

function of the signal. These points define a symmetric structure around the vertical axis, originating at the natural frequency of 1000 Hz. The dimensions of the axes of the rhombs are 100 Hz in the vertical direction and 50 Hz in the horizontal direction, clearly indicating a modulation with the rotation frequency of 25 Hz. The spacing of the centres of the rhombs is 266 Hz in the vertical direction and 133 Hz in the horizontal direction, clearly indicating a further modulation with the BPFI frequency of 133 Hz.

4. EXPERIMENTAL RESULTS

Two characteristic cases are presented, each one being typical of a different type of bearing fault. In all cases, the measuring device is based on a Pentium II/266 MHz portable computer, equipped with a PCMCIA DAQCard-1200 data acquisition card from National Instruments. This is an 8-channel software-configurable 12-bit data acquisition card, with a total sampling rate capacity of 100 kHz. A B&K-type 8325 accelerometer is used, with a sensitivity of 97·3 mV/g and a dynamic range of 1 Hz to 10 kHz. The code of the algorithm that is used in the data acquisition procedure and signal analysis has been developed under the LabVIEW programming environment of National Instruments and the signal analysis was accomplished with the aid of the MATLAB signal processing toolbox.

The measurements in Case A were conducted on a fan motor with an outer race bearing fault at the industrial installation of Aluminium of Greece S.A. The shaft rotation speed during the measurement was around 1500 r.p.m. The bearing monitored is SKF type 6324MC3, with a BPFO frequency equal to 3·13 times the shaft rotation speed, leading to a theoretical estimation of the expected BPFO frequency around 78 Hz. The measured signal is shown in Figure 10 and its PSD is shown in Figure 11. A number of peaks appear in the area between 2000 Hz and 3200 Hz. Figure 12 presents the DCS function of the signal. Similar to the typical pattern in Figure 4, it is characterized by the presence of a number of non-zero cycle frequencies A1–A5, corresponding, respectively, to the BPFO frequency of the signal and its harmonics.

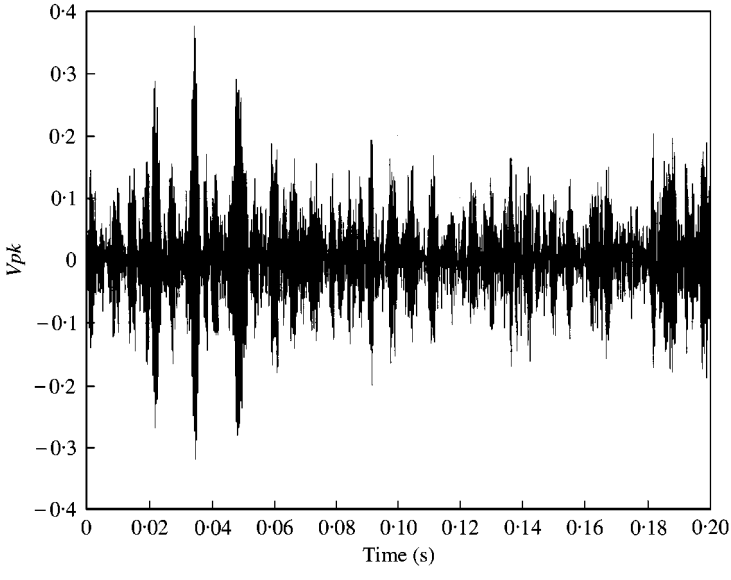

Figure 10. Vibration signal measured in Case A (outer race bearing fault).

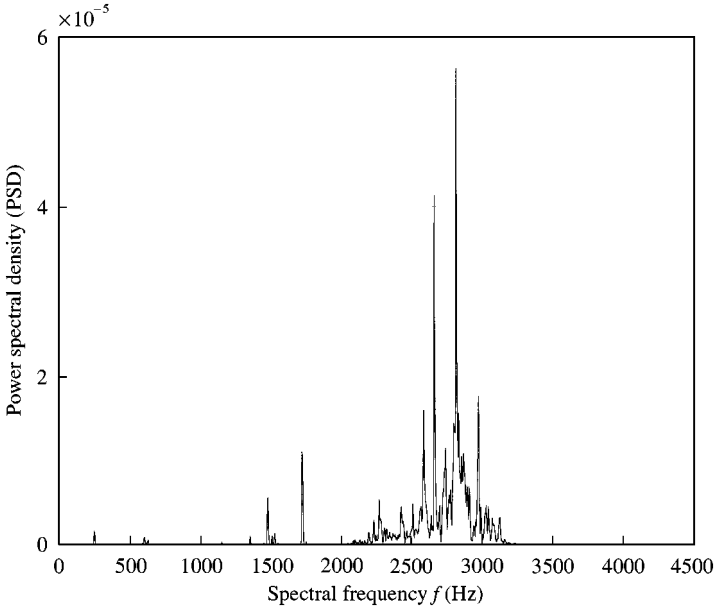

Figure 11. Power spectral density of the signal in Figure 10 (Case A, outer race bearing fault).

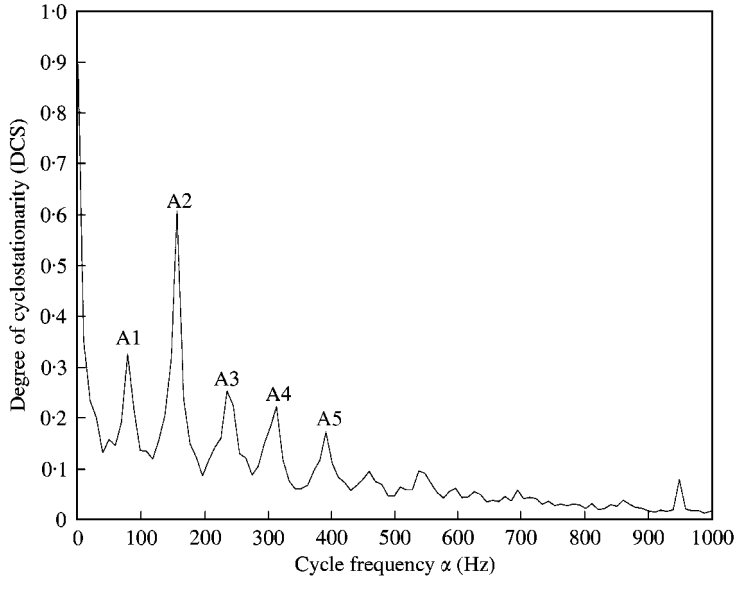

Figure 12. Degree of cyclostationarity function of the signal in Figure 10 (Case A, outer race bearing fault).

Figure 13 shows the SCDF of the signal, as presented in the area between 2500 Hz and 3200 Hz in the spectral frequency f-axis and between 0 and 600 Hz in cycle frequency α-axis. Similar to the pattern appearing in Figure 5, the SCDF is characterized by distinct points in a symmetric rhombic structure around the vertical axis, originating at the frequency of 2820 Hz (presumably representing a natural frequency of the system). The spacing of the points is about 160 Hz in the vertical direction and 80 Hz in the horizontal direction, clearly characterizing a modulation effect by the BPFO frequency.

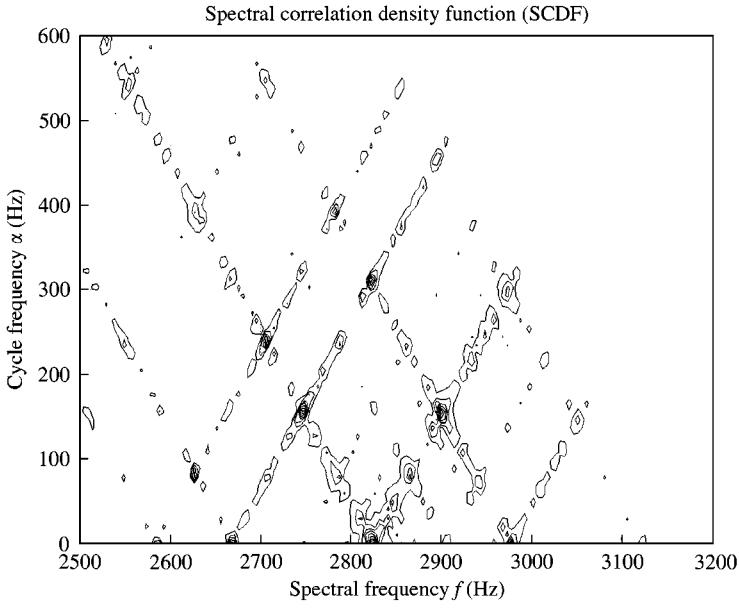

Figure 13. Spectral correlation density function of the signal in Figure 10 (Case A, outer race bearing fault).

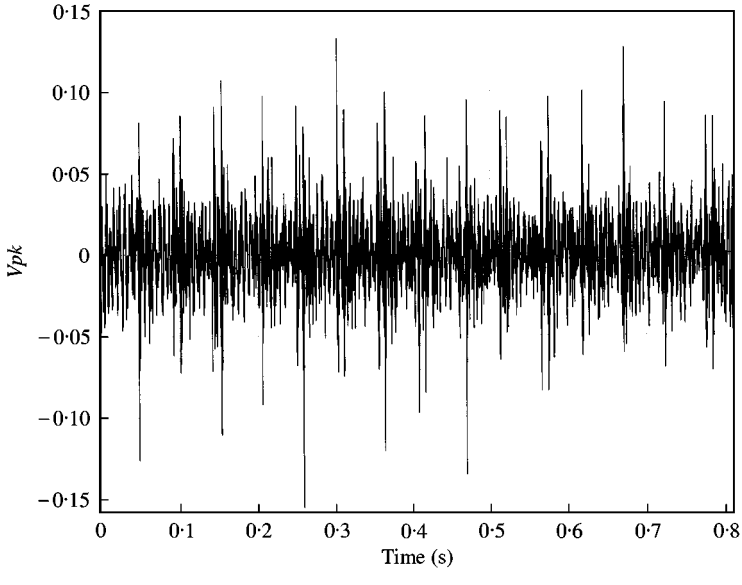

Figure 14. Vibration signal measured in Case B (inner race bearing fault).

The measurements in Case B were conducted on a machinery fault simulator manufactured by SpectaQuest on a bearing presenting an inner race fault. The shaft rotation speed during the measurement was around 1200 r.p.m. The bearing monitored is SKF type 7303BEP, with a BPFI frequency equal to 5·53 times the shaft rotation speed, leading to a theoretical estimation of the expected BPFI frequency around 110 Hz. The measured signal is shown in Figure 14 and its PSD is shown in Figure 15, showing a large

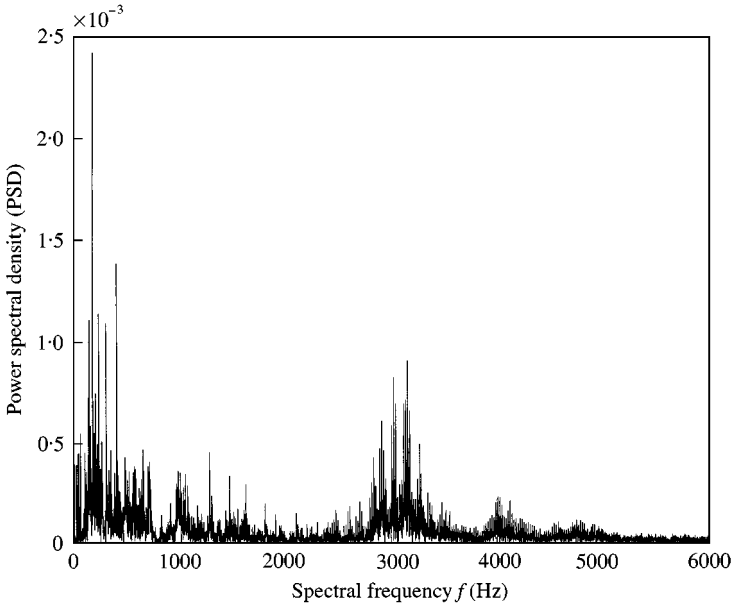

Figure 15. Power spectral density of the signal in Figure 14 (Case B, inner race bearing fault).

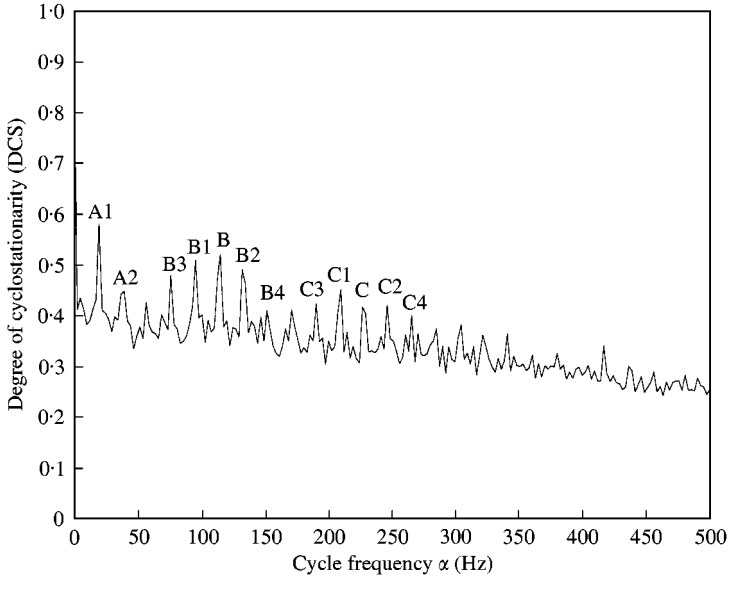

Figure 16. Degree of cyclostationarity function of the signal in Figure 14 (Case B, inner race bearing fault).

number of distinct frequencies. The signal is then band-pass filtered in the area 2500–3500 Hz and further processed by cyclostationary analysis. The DCS function of the band-pass filtered signal is shown in Figure 16. A large number of distinct cycle frequencies appear. The most important ones correspond to the shaft rotation speed and its second harmonic (points A1, A2, respectively) to the BPFI frequency and its second harmonic (points B, C, respectively) and to sidebands around them (points B1–B2/B3–B4,

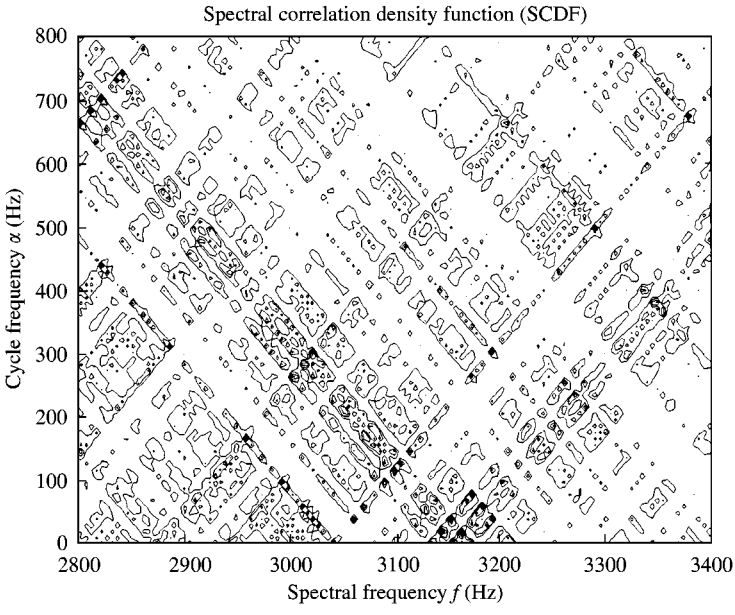

Figure 17. Spectral correlation density function of the signal in Figure 14 (Case B, inner race bearing fault).

C1–C2/C3–C4, respectively), corresponding to frequencies equal to the shaft rotation speed and its second harmonic.

Figure 17 shows the SCDF of the filtered signal, as presented in the area between 2800 Hz and 3400 Hz in the spectral frequency f-axis and between 0 and 800 Hz in the cycle frequency α-axis. A complex rhombic structure appears, with vertical and horizontal spacing of points corresponding primarily to multiples of the shaft rotation speed. Secondarily, multiples of the BPFI frequency and of its sums and differences with the rotation frequency can be observed.

The DCS function (Figure 16) and the SCDF (Figure 17) of the measured signal, compared to their corresponding typical patterns in Figures 8 and 9 of the simulated signal, are far more complex in structure. This is due to the fact that the modulation mechanism present in the measured signal is far stronger and more complex than that of the simulated one. Furthermore, it is dominated mainly by the shaft rotation frequency and secondarily by the BPFI frequency. This type of response is quite common in bearings with inner race faults, when the wear is severe and/or not all the bearing balls excite the loading zone to the same extent. Although more complicated than the case of an outer race fault, both the DCS and the SCDF functions contain the typical patterns which provide a clear evidence of the inner race fault.

5. CONCLUSION

The framework offered by cyclostationary analysis can provide a wide variety of tools, which are more efficient than those of traditional spectral analysis with respect to the exhibition and verification of the various physical modulation mechanisms present in rolling-element bearings vibration response. The degree of cyclostationarity (DCS) function can provide a first overall indication of the appearance of several distinct modulating frequencies. Although equally simple in its presentation form to the PSD of the envelope of

the signal, it offers additionally a number of advantages concerning its effectiveness and computation. Further details and confirmation of the exact form of the various modulation mechanisms present can be derived by the spectral correlation density function (SCDF) of the signal, which are far more detailed in content than the traditional power spectral density. Specific types of bearing faults can be characterized by "typical frequency patterns" in the DCS and SCDF functions, as indicated in the simulated signals and verified to a satisfactory degree in corresponding measured signals. Additional methods within the framework of cyclostationary analysis as well as other complementary pattern classification and data reduction methods can further exploit the information content made available by cyclostationary analysis.

ACKNOWLEDGMENT

This work has been supported in part by a grant from the General Secretariat of Research and Technology, Greek Ministry of Development.

REFERENCES

1. N. TANDON and A. CHOUDHURY 1999 *Tribology International* **32**, 469–480. A review of vibration and acoustic measurement methods for the detection of defects in rolling element bearings.
2. P. D. MCFADDEN and J. D. SMITH 1984 *Journal of Sound and Vibration* **96**, 69–82. Model for the vibration produced by a single point defect in a rolling element bearing.
3. A. CHOUDHURY and N. TANDON 1998 *American Society of Mechanical Engineers Journal of Vibration and Acoustics* **120**, 214–220. A theoretical model to predict vibration response of rolling bearings to distributed defects under radial load.
4. Y. SU, M. H. LIN and M. S. LEE 1993 *Journal of Sound and Vibration* **165**, 455–466. The effects of surface irregularities on roller bearing vibrations.
5. C. S. SUNNERJO 1985 *Journal of Sound and Vibration* **98**, 455–474. Rolling bearing vibrations—The effects of geometrical imperfections and wear.
6. R. B. RANDALL 1987 *Frequency Analysis*. Naerum, Denmark: Bruel & Kjaer; third edition.
7. J. C. LI and J. MA 1997 *NDT&E International* **30**, 143–149. Wavelet decomposition of vibrations for detection of bearing-localized defects.
8. K. MORI, N. KASASHIMA, T. YOSHIOKA and Y. UENO 1996 *Wear* **195**, 162–168. Prediction of spalling on a ball bearing by applying the discrete wavelet transform to vibration signals.
9. R. RUBINI and U. MENEGHETTI 1998 *Proceedings of the Third International Conference on Acoustical and Vibratory Surveillance Methods and Diagnostic Techniques*, *Senlis*, *France*, 371–378. Use of the wavelet transform for the diagnosis of incipient faults in ball bearings.
10. W. A. GARDNER 1994 in *Cyclostationarity in Communications and Signal Processing* (W. A. Gardner, editor). NJ, U.S.A.: IEEE Press; Chapter 1. An introduction to cyclostationary signals.
11. G. B. GIANNAKIS 1999 *The Signal Processing Handbook*. Boca Raton, FL: CRC Press and New York: IEEE Press; Chapter 17.
12. C. CAPDESSUS, M. SIDAHMED and J. L. LACOUME 2000 *Mechanical Systems and Signal Processing* **14**, 371–385. Cyclostationary processes: application in gear faults early diagnosis.
13. A. C. MCCORMIC and A. K. NANDI 1998 *Mechanical Systems and Signal Processing* **12**, 225–242. Cyclostationarity in rotating machine vibrations.
14. R. S. ROBERTS, W. A. BROWN and H. H. LOOMIS JR. 1994 in *Cyclostationarity in Communications and Signal Processing* (W. A. Gardner, editor). NJ, U.S.A.: IEEE Press; Article 6. A review of digital spectral correlation analysis: theory and implementation.